UDC 551.509.313

A Vertically Integrated Primitive-Equation Model

JOSEPH SELA and WILLIAM J. BOSTELMAN—*National Meteorological Center, National Weather Service, NOAA, Suitland, Md.*

ABSTRACT—The primitive equations are integrated with respect to the vertical coordinate, sigma. The resulting equations contain vertical eddy terms arising from nonlinearities. These eddies are parameterized using a standard-atmosphere temperature distribution and a linear jet wind profile independent of horizontal position. The model includes topography and is capable of responding to diabatic heating. Experiments with and without the continuity equation are carried out, and a comparison is made with barotropic forecasts. Exclusion of the mass continuity condition results in superior forecasts, especially near high terrain.

1. INTRODUCTION

The trend in numerical weather prediction (NWP) has been, and most likely will continue to be, in the direction of increased resolution in both the horizontal and vertical coordinates. The motivation behind this trend is the conviction that finer resolutions lead to improved accuracy in the description of the atmosphere's initial state as well as to more accurate prediction models. The practical problems of NWP for periods beyond the short range necessitate a compromise between the amount of predicted information and practical constraints. One way to achieve the simplification and economy required for long computer runs is to sacrifice knowledge of the vertical structure. For practical extended and long-range predictions, this loss is tolerable; expecially since such results may have to be interpreted in a somewhat statistical sense. It can be also argued that the prediction of the vertically integrated temperature and wind is a relatively simpler task than the prediction of their vertical variation.

Integrating out the vertical dependence results in primitive equations that contain momentum and heat transports, which arise from nonlinearities and which are functions of time and horizontal position only. These transports can be expressed in terms of the vertical means and of the integrals of products of deviations from those means, referred to as eddies in this study. To close the problem, we must parameterize these eddies. To this end, we prescribe a standard-atmosphere lapse rate and use a simple, dual linear, jetlike wind law. We also consider the energy budget, thus enabling the model to respond to diabatic heating, unlike the one-level barotropic model.

The integration domain for longer periods of time should ideally be global. However, in this preliminary study of the practicality of the vertically integrated approach, the domain chosen was the rectangular, quasi-hemispheric domain presently used at the National Meteorological Center.

2. FORMULATION

We consider the hydrostatic version of the conservation of momentum, mass, and energy on a polar stereographic map projection using Phillips' (1957) vertical coordinate system.

Using the conventional notation, we may write the equations as follows:

$$\frac{\partial u}{\partial t}+m\mathbf{V}\cdot\nabla u+\dot{\sigma}\frac{\partial u}{\partial \sigma}=f^*v-m\left(\phi_x-\frac{\sigma}{\pi}\frac{\partial \phi}{\partial \sigma}\pi_x\right) \tag{1}$$

$$\frac{\partial v}{\partial t}+m\mathbf{V}\cdot\nabla v+\dot{\sigma}\frac{\partial v}{\partial \sigma}=-f^*u-m\left(\phi_y-\frac{\sigma}{\pi}\frac{\partial \phi}{\partial \sigma}\pi_y\right) \tag{2}$$

$$\frac{\partial \phi}{\partial \sigma}=-\frac{RT}{\sigma} \tag{3}$$

$$\frac{\partial \pi}{\partial t}+\pi\frac{\partial \dot{\sigma}}{\partial \sigma}+m^2\nabla\cdot\frac{\pi\mathbf{V}}{m}=0 \tag{4}$$

and

$$\frac{\partial \theta}{\partial t}+m\mathbf{V}\cdot\nabla\theta+\dot{\sigma}\frac{\partial \theta}{\partial \sigma}=\frac{\theta H}{c_pT} \tag{5}$$

where

f is the Coriolis parameter,
$f^*=f-vm_x+um_y$,
H is heating rate,
m is map factor,
p is pressure,
R is specific gas constant,
(u, v) are the horizontal wind components,
$\mathbf{V}$ is the vector wind,
θ is potential temperature,
π is surface pressure,
$\sigma=\frac{p}{\pi}$,/the vertical coordinate,

and

ϕ is geopotential.

To eliminate the explicit dependence on the vertical

529-411 O - 74 - 5

coordinate σ, we define the operator

$$\hat{(\ )}=\int_0^1 (\ )d\sigma \tag{6}$$

and apply it to eq (1)–(5), after splitting all variables according to $(\ )=\hat{(\ )}+(\ )'$. We obtain

$$\frac{\partial\hat{u}}{\partial t}=\hat{v}(f-m_x\hat{v}+m_y\hat{u})-m\hat{\mathbf{V}}\cdot\nabla\hat{u}$$
$$-mR\left(\hat{T}_x+\frac{\hat{T}\pi_x}{\pi}\right)-m\phi_x(1)+u_E, \tag{7}$$

$$u_E=m_x(\hat{u'^2}-\hat{v'^2})+2m_y\widehat{u'v'}-m\nabla\cdot\widehat{u'\mathbf{V}'}-\frac{\widehat{mu'\mathbf{V}'}}{\pi}\cdot\nabla\pi, \tag{8}$$

$$\frac{\partial\hat{v}}{\partial t}=-\hat{u}(f-m_x\hat{v}+m_y\hat{u})-m\hat{\mathbf{V}}\cdot\nabla\hat{v}$$
$$-mR\left(\hat{T}_y+\frac{\hat{T}\pi_y}{\pi}\right)-m\phi_y(1)+v_E, \tag{9}$$

$$v_E=-m_y(\hat{u'^2}-\hat{v'^2})+2m_x\widehat{u'v'}-m\nabla\cdot\widehat{v'\mathbf{V}'}-\frac{\widehat{mv'\mathbf{V}'}}{\pi}\cdot\nabla\pi, \tag{10}$$

$$\frac{\partial\pi}{\partial t}=-m^2\nabla\cdot\frac{\pi\hat{\mathbf{V}}}{m}, \tag{11}$$

$$\frac{\partial\hat{T}}{\partial t}=\frac{1}{c_p}(\hat{H}+C_E)-m\hat{\mathbf{V}}\cdot\nabla\hat{T}-m\nabla\cdot\widehat{T'\mathbf{V}'}-\frac{m^2}{\pi}\widehat{T'\mathbf{V}'}\cdot\nabla\frac{\pi}{m}, \tag{12}$$

and

$$C_E=R\int_0^1 T\left[\frac{1}{\pi}\left(\frac{\partial\pi}{\partial t}+m\mathbf{V}\cdot\nabla\pi\right)+\frac{\dot{\sigma}}{\sigma}\right]d\sigma. \tag{13}$$

In eq (7) and (9), we used the integrated hydrostatic equation $\hat{\phi}=\phi(1)+R\hat{T}$, where $\phi(1)$ is the geopotential at the surface of the earth. Boundary conditions $\dot{\sigma}=0$ at $\sigma=0$ and $\sigma=1$ were also used.

Equations (7)–(13) contain "eddy" terms $\widehat{u'\mathbf{V}'}$, $\widehat{v'\mathbf{V}'}$, and $\widehat{\mathbf{V}'T'}$, which must be specified to close the system. An estimate of the magnitude of these terms can be obtained either by computing them from observed data or by integrating a simple model atmosphere. Both computations were made, with the result that the horizontal heat transport carried by the "vertical eddies" is only a few percent of the heat transport produced by the mean flow, but the horizontal momentum eddy transport is appreciable.

The first experiments using the integrated equations were conducted by specifying the eddy quantities from observations. Long-term normal values of winds and temperature given at 11 levels (up to 50 mb) were used to obtain normal eddies. These eddies were then held constant during the integration. The results of this approach were not satisfactory. Since the observed eddy quantities are variable in time, the adjustment of any initial wind and temperature conditions to incompatible eddies results in a poor forecast with large-amplitude distortions, particularly near high terrain.

The second series of experiments was conducted by

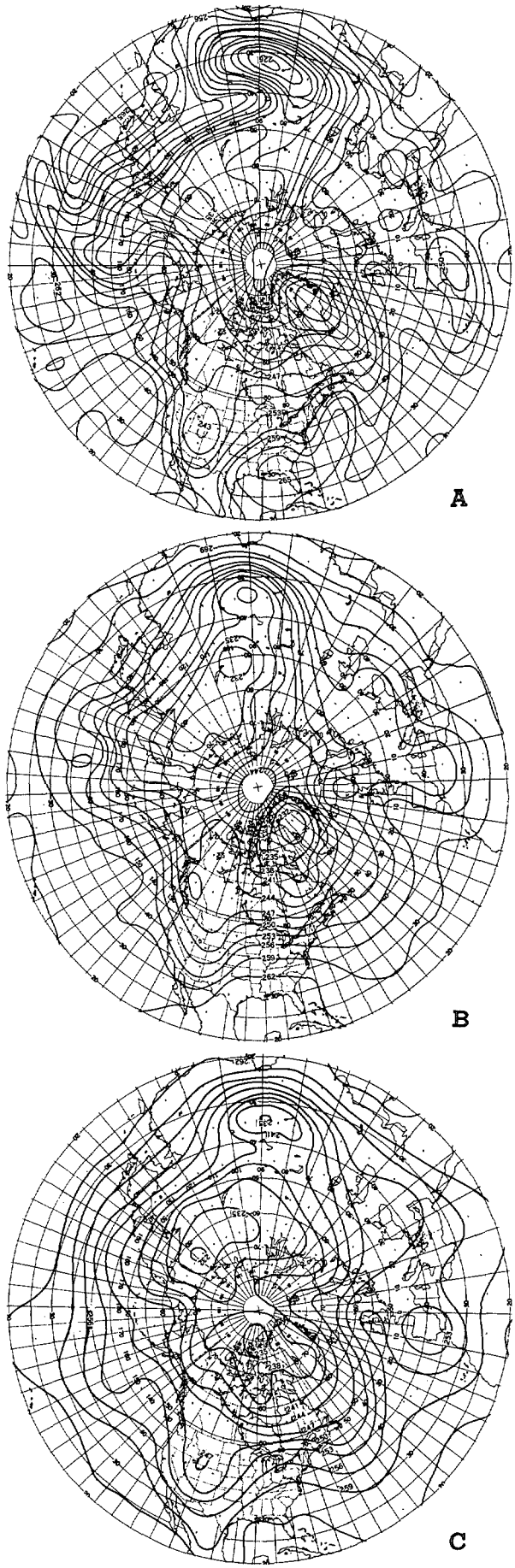

FIGURE 1.—(A) set I 72-hr predicted ($\partial\pi/\partial t\neq 0$), (B) set II 72-hr predicted ($\partial\pi/\partial t=0$), and (C) observed mean temperature (°K) maps for 1200 GMT, Nov. 2, 1972. Contours are at 3°K intervals.

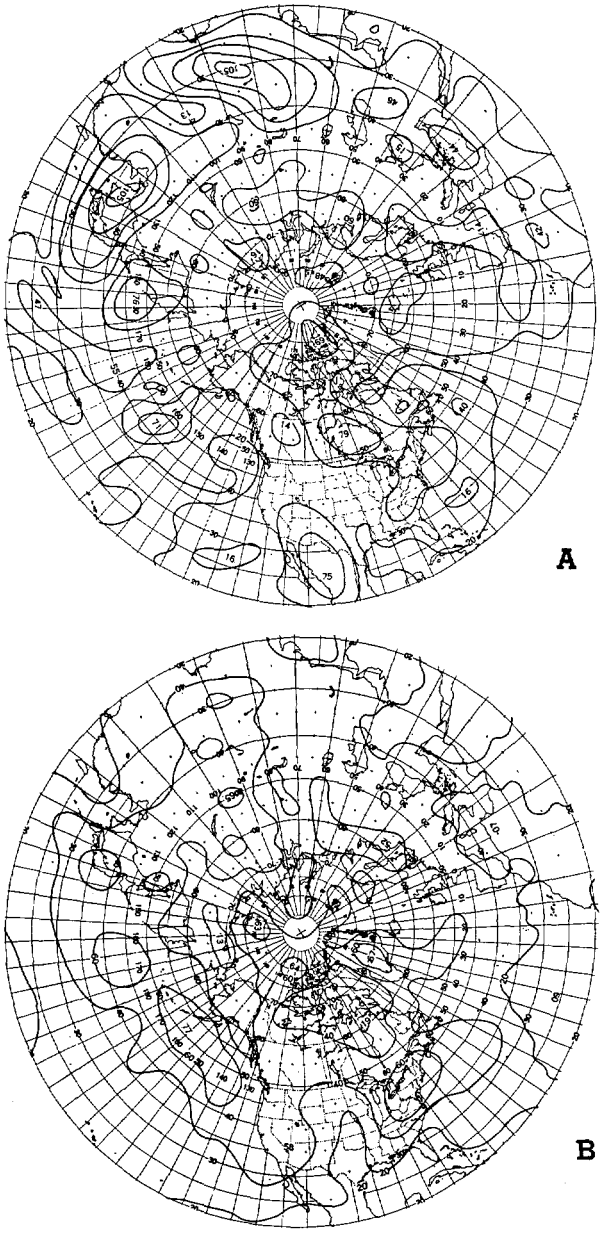

FIGURE 2.—The 72-hr rms error maps of mean temperature (tens of °K) for (A) set I (five cases from Oct. 1–30, 1972) and (B) set II (five cases from Nov. 1–30, 1972). The contour interval is 200°K.

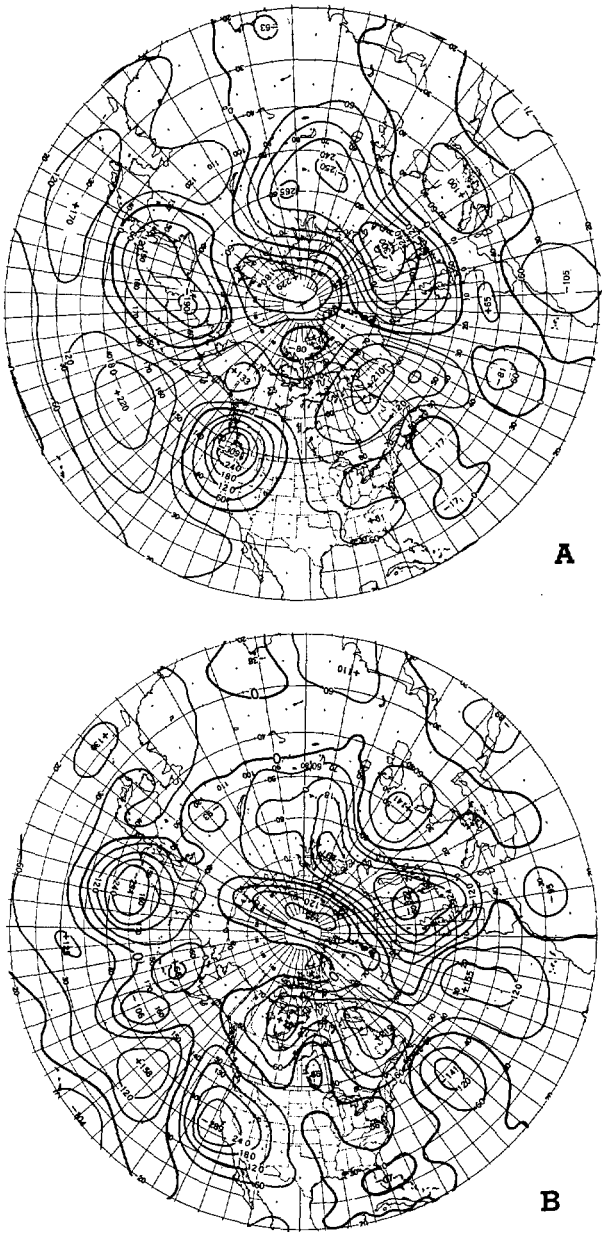

FIGURE 3.—Departures from normal 500-mb height fields (m) of (A) 72-hr values predicted by the barotropic model and (B) observed values at 1200 GMT, Nov. 11, 1972. Contours are at 60-m intervals.

prescribing a wind law of the form

$$\mathbf{V}=A(\sigma)\hat{\mathbf{V}} \tag{14}$$

where

$$A(\sigma)=\begin{cases}\dfrac{2\sigma}{\sigma_T} & 0\le\sigma\le\sigma_T\\[2ex] 2\,\dfrac{1-\sigma}{1-\sigma_T} & \sigma_T\le\sigma\le 1\end{cases} \tag{15}$$

and $\sigma_T=0.2$.

The temperature profile was taken as

$$T=B(x, y, \sigma)\ \hat{T} \tag{16}$$

where B is defined at every point of the map by the standard-atmosphere value of $\hat{T}$, as influenced by the underlying terrain.

Using this parameterization, we get the following prognostic equations:

$$\frac{\partial\hat{u}}{\partial t}=m\left[(1-\hat{A}^2)\hat{u}\left(m\nabla\cdot\frac{\hat{\mathbf{V}}}{m}+\frac{\hat{\mathbf{V}}}{\pi}\cdot\nabla\pi\right)-\hat{A}^2\hat{\mathbf{V}}\cdot\nabla\hat{u}\right.$$
$$\left.-\phi_x(1)-R\hat{T}_x-\frac{R\hat{T}}{\pi}\pi_x\right]+\hat{v}[f-\hat{A}^2(\hat{v}m_x-\hat{u}m_y)], \tag{17}$$

$$\frac{\partial\hat{v}}{\partial t}=m\left[(1-\hat{A}^2)\hat{v}\left(m\nabla\cdot\frac{\hat{\mathbf{V}}}{m}+\frac{\hat{\mathbf{V}}}{\pi}\cdot\nabla\pi\right)-\hat{A}^2\hat{\mathbf{V}}\cdot\nabla\hat{v}\right.$$
$$\left.-\phi_y(1)-R\hat{T}_y-\frac{R\hat{T}}{\pi}\pi_y\right]-\hat{u}[f-\hat{A}^2(\hat{v}m_x-\hat{u}m_y)], \tag{18}$$

$$\frac{\partial\pi}{\partial t}=-m^2\nabla\cdot\frac{\pi\hat{\mathbf{V}}}{m}, \tag{19}$$

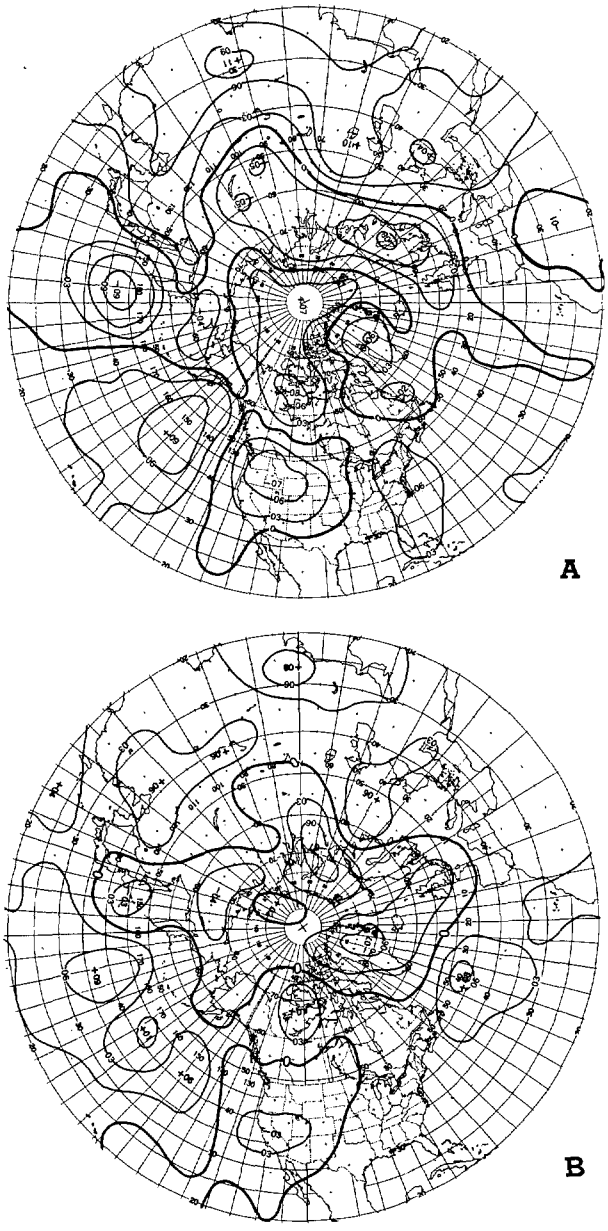

FIGURE 4.—Departures from normal mean temperature fields (°K) of (A) 72-hr values predicted for set II ($\partial\pi/\partial t=0$) and (B) observed values at 1200 GMT, Nov. 11, 1972. Contours are at 3° intervals.

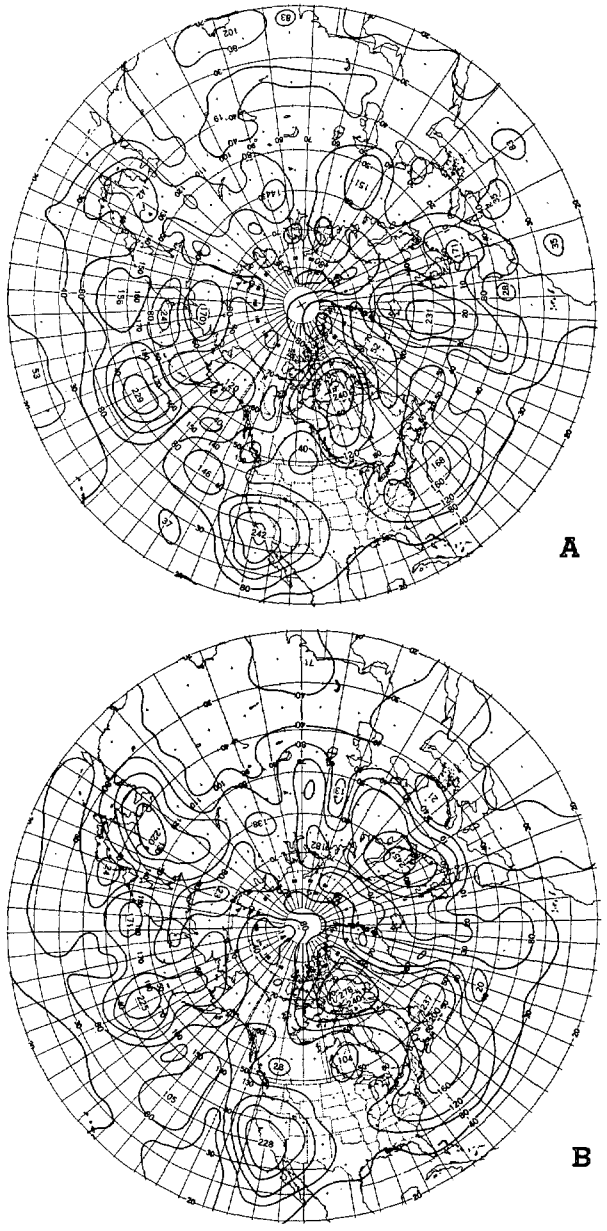

FIGURE 5.—(A) the 72-hr rms error map of predicted 500-mb height DNs and (B) the observed rms 500-mb height DN map (m). Contours are at 40-m intervals. A three-case average is used here.

and

$$\frac{\partial\hat{T}}{\partial t}=s_1 m^2 T\nabla\cdot\frac{\hat{\mathbf{V}}}{m}+s_2\frac{m\hat{T}\hat{\mathbf{V}}}{\pi}\cdot\nabla\pi$$

$$-m\widehat{AB}\hat{\mathbf{V}}\cdot\nabla\hat{T}-m\hat{T}\hat{\mathbf{V}}\cdot\nabla\widehat{AB}, \quad (20)$$

where

$$s_1=1-\kappa\,\widehat{BD}-\widehat{AB}, \quad (21)$$

$$s_2=1-\kappa\,\widehat{BD}-\widehat{AB}(1-\kappa), \quad (22)$$

$$D(\sigma)=\frac{1}{\sigma}\int_0^\sigma A\,d\sigma,$$

and

$$\kappa=\frac{R}{c_p}.$$

Since the objective of these experiments is to determine whether the integrated approach has any validity for prediction purposes beyond the short range, we felt that realistic topography should be incorporated from the outset. For this purpose, slightly smoothed mountains were used, the highest points on the map being 4.5 km.

Initial conditions for eq (17)–(20) are obtained by vertically integrating 10 levels of wind and temperature data, reaching 100 mb. The surface pressure is obtained hydrostatically by considering the topography and a standard-atmosphere lapse rate; that is,

$$\pi=p_0\left(1-\frac{\gamma z}{T_0}\right)^{g/\gamma R}+P_{s1}-p_0.$$

Here, p_0 and T_0 are the standard sea-level pressure and temperature, g is gravity, z is the surface height above sea

level, and γ is the lapse rate. This specification of surface pressure was found necessary to produce geostrophically compatible surface pressure topography and temperature. P_{sl} is the observed sea-level pressure.

Two sets of experiments were conducted, one with the full set of eq (17)–(20), the other with constant surface pressure (i.e., $\partial\pi/\partial t=0$). A time step of 10 min is used in the centered time differencing scheme, well within the linear stability criterion for gravitational phase speeds inherent in the model (these are found to be $c^2=\kappa \hat{RT}$).

While no initialization procedure was required for the constant surface pressure case, the same initial data used with the full set of equations gave rise to considerable amplitude oscillations of periods around 10 hr. To combat these unwanted distortions and still keep the initialization procedure as simple as possible, we averaged the first 10 hr of integration; the initial time for these runs should be considered to be t_0+5 hr.

To maintain stability, we used a time filter (Asselin 1972) of the form

$$F^{(n)}=\alpha F_*^{(n)}+\frac{1-\alpha}{2}[F_*^{(n+1)}+F^{(n-1)}]$$

where $\alpha=0.95$ is the damping and n is the time index. In addition, we applied a spatial low-pass smoother every 24 hr.

3. RESULTS

Experimental 36- and 72-hr forecasts were made with the model for five cases of set I [with eq (19)] and set II [without eq (19)]. Observed data from the November–December 1972 period were used as input. As a comparison, a version of the barotropic model that predicts 500-mb heights was run concurrently with each set. Since the mean temperature predicted by the model has a positive correlation to mean height, this comparison can be made. Departures from normal (DN) and root mean square (rms) errors were computed for the respective models. The rms errors were then averaged over each set of five cases.

Evaluation of the results will focus on the comparison of the rms errors and of the behavior of the DNs. The discussion of these will be divided into two parts and limited to the 72-hr predictions. Part 1 will compare the results of set I with set II; part 2 will compare the results of set II with the barotropic model.

Part 1: Comparison of Set I with Set II

A November 1 case for set I and set II starting at the same initial time (1200 GMT) is shown in figure 1. When figure 1A (set I) is compared to the observed state (fig. 1C), it is apparent that the predicted large-scale mean temperature pattern is distorted and overly developed. In addition, many small-scale features and extremely large gradients (especially in mountainous areas) in the predicted field (fig. 1A), were not observed. Figure 1B (set II), however, seems to reasonably represent the large-scale temperature pattern in terms of shape and magnitude. Furthermore, the gradients in figure 1B approach reality, and the small-scale features are notably fewer than in figure 1A.

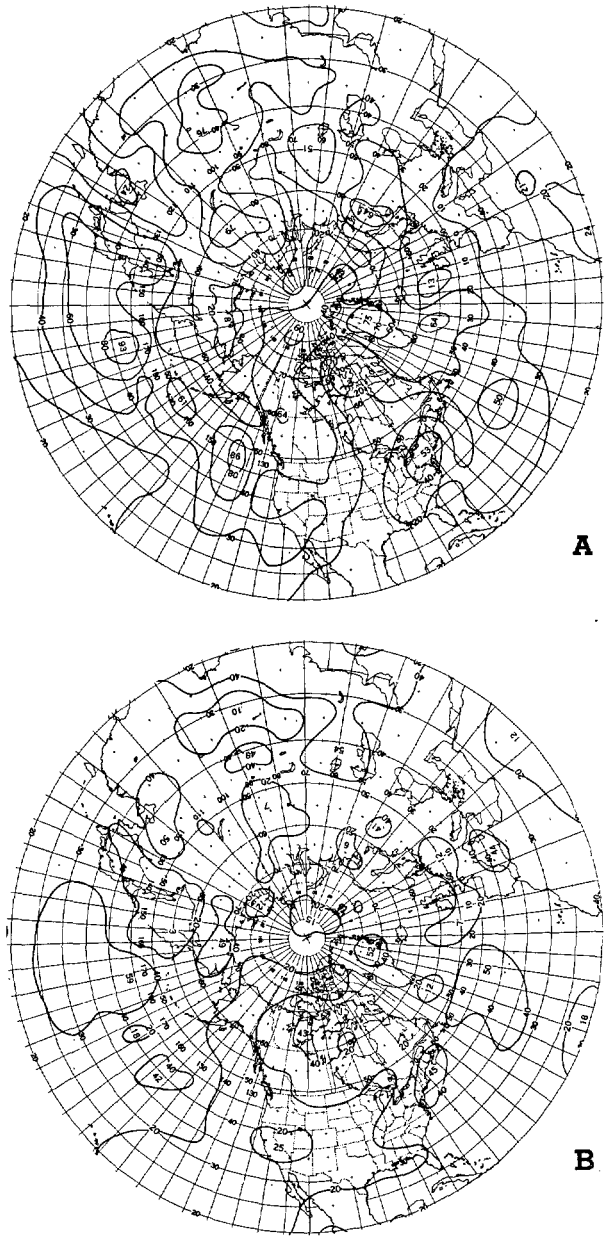

FIGURE 6.—(A) the 72-hr rms error map of predicted mean temperatures from set II and (B) the observed rms mean temperature DN map (tens of °K). The contour interval is 200°K. A three-case average is used here.

Examination of the rms temperature error maps from each set (fig. 2) shows that both set I and set II have difficulties forecasting near and over mountain ranges. A study of individual cases has shown a tendency for the model to predict temperatures too high east of mountain ranges and too low over the mountains. Results similar to those in figure 2 (five-case average) were obtained by Miyakoda et al. (1972). In that paper, the 500-mb temperature errors for 1- to 4-day forecasts were largest over data-sparse regions at middle latitudes.

Part 2: Comparison of Set II With Barotropic (3 cases)

A November 8 case (initial time, 1200 GMT) is presented in figures 3 and 4. Observed and forecast DNs (500-mb height and temperature) for 72 hr after the initial time are shown. As can be seen from these maps, the models behave quite differently. The barotropic model (fig. 3) has trough and ridge systems that generally move too slowly and are underdeveloped. Set II forecasts (fig. 4), however, indicate movement and magnitude of systems that are, on the average, greater than observed.

Another difference between the two models can be seen by comparing the rms DN error maps with the observed rms DN maps (figs. 5, 6). Comparison of figures 5A and 5B shows that the areas of large height DN errors of the barotropic model are associated with areas of large observed height DNs. No such correlation is indicated between the temperature maps (figs. 6A, 6B).

Finally, to measure the performance of set II against that of the barotropic model, we averaged the rms observed DNs and rms DN errors over the entire map and then compared them. Both models' average rms DN error was significantly less than their average observed rms DN at 36 hr and within 10 percent of it at 72 hr.

4. SUMMARY

The vertically integrated model, which excludes the continuity equation, performs satisfactorily out to 72 hr. It has some problems over the Pacific Ocean and in areas of high terrain. Nevertheless, the results indicate that its skill is at least equal to that of the barotropic model—it may even be superior to it at 72 hr. The subordination of the motion to the energy constraint only, rather than to the conservation of mass and energy, is an attractive feature since it allows the inclusion of diabatic heating in a barotropic framework. Continued work, including the consideration of heating and friction, is desirable.

REFERENCES

Asselin, Richard, "Frequency Filter for Time Integrations," *Monthly Weather Review*, Vol. 100, No. 6, June **1972**, pp. 487–490.

Miyakoda, K., Hembree, G. D., Strickler, R. F., and Shulman, I., "Cumulative Results of Extended Forecast Experiments: I. Model Performance for Winter Cases," *Monthly Weather Review*, Vol. 100, No. 12, Dec. **1972**, pp. 836–855.

Phillips, Norman A., "A Coordinate System Having Some Special Advantages for Numerical Forecasting," *Journal of Meteorology*, Vol. 14, No. 2, Apr. **1957**, pp. 184–185.

[*Received April 10, 1973; revised October 16, 1973*]